



# Investigations on Fe doped SnS thin films by nebulizer spray pyrolysis technique for solar cell applications

S. Sebastian<sup>1</sup> · I. Kulandaisamy<sup>1</sup> · S. Valanarasu<sup>1</sup> · N. Soundaram<sup>2</sup> · K. Paulraj<sup>3</sup> · Dhanasekaran Vikraman<sup>4</sup> · Hyun-Seok Kim<sup>4</sup>

Received: 7 January 2019 / Accepted: 11 March 2019 / Published online: 18 March 2019  
© Springer Science+Business Media, LLC, part of Springer Nature 2019

## Abstract

Undoped and different concentrations of iron (Fe) doped tin sulphide (SnS) thin films were coated by nebulizer spray pyrolysis method with the substrate temperature of 350 °C. Polycrystalline nature of orthorhombic crystal structured pure and Fe doped SnS (Fe:SnS) thin films confirmed by X-ray diffraction (XRD) patterns. Structural studies further explored the preferential orientation of (201) plane for undoped SnS and their shifts to (400) and (111) directions for Fe:SnS at 6 and 10 wt.% of Fe concentration, respectively. The versatile route of structural modification has obviously demonstrated due to inclusion of Fe doping in SnS. Raman spectra further confirmed the structural variation of Fe:SnS. Topological variations obviously explained by atomic force microscopy images for pure and Fe:SnS. Optical results evidently claimed the deterioration of band gap values from 1.96 to 1.58 eV due to increase of Fe doping concentrations from 0 to 10 wt.%, respectively. Luminescence spectra showed a strong emission peak centered at 772 nm and low resistivity  $3.32 \times 10^{-2} \Omega \text{ cm}$  with the high carrier concentration for 8 wt.% of Fe concentration using prepared Fe:SnS film. The fabricated solar cell device with n-CdS exposed the 0.18% of efficiency for p-Fe:SnS prepared using 8 wt.% Fe concentration.

## 1 Introduction

A semiconductor compound under the classification of IV–VI group is extensively used owing to their strong electronic correlations [1–3]. Recently, research community have paid great attention on tin sulfide (SnS) thin film, which is from the group of IV-VI, non-toxic and naturally abundant, because it has a *p*-type properties and high absorption co-efficient with orthorhombic crystal structure [3–5]. These properties make it attractive as a selective solar absorber material for the heterojunction solar cells [6]. In addition, SnS is highly attracted due to their broad range of feasibility to use different applications such as optoelectronic devices,

light emitting diodes, high-power lithium ion batteries, photo-conductive, gas and chemical sensors and pigments [7–11]. The numerous techniques were employed to prepare SnS films such as RF-sputtering [12], thermal evaporation [13], electron beam evaporation [14], SILAR method [15], chemical bath deposition [16], electro deposition [17] and spray pyrolysis [19, 30]. Among these techniques, nebulized spray technique (NSP) is an efficient and cost effective route to fabricate SnS thin films on different substrates [18].

From the available literatures, some metals like, lead [19], aluminium [20], copper [21], silver [22], antimony [23], and indium [24] have been doped with SnS films to improve the opto-electronic properties. Among them, ferrous (Fe) is one of the potential dopant element with SnS and their impurity states claims the Fermi level make possible to transfer of electrons between CB and VB [25]. Since the ionic radius of  $\text{Fe}^{2+}$  (0.76 Å) is lower than the ionic radius of  $\text{Sn}^{2+}$  (0.93 Å), the  $\text{Sn}^{2+}$  ions can be effectively replaced by  $\text{Fe}^{2+}$  ions without causing any real change in crystalline nature and lattice parameters [26]. So doping at the Sn vacancy sites in the SnS lattice alters the acceptor density and modifies the resistivity. The preferred density for developing the photovoltaic performance are in the range from  $10^{15}$  to  $10^{19} \text{ cm}^{-3}$ , so optimization of the doping concentration is more important for

✉ S. Sebastian  
speedseba@yahoo.co.in

<sup>1</sup> PG& Research Department of Physics, Arul Anandar College, Karumathur, Madurai, Tamil Nadu 625 514, India

<sup>2</sup> Department of Physics, Sree Sevugan Annamalai College, Devakottai 630303, India

<sup>3</sup> Department of Physics, Pasumpon Muthuramalinga Thevar College, Usilampatti, India

<sup>4</sup> Division of Electronics and Electrical Engineering, Dongguk University-Seoul, Seoul 04620, Republic of Korea

obtaining the suitable acceptor density of SnS films [27]. For a potential photovoltaic, as an absorber layer of SnS thin film has an optimal band gap. In any case, it might be conceivable to change the vitality band gap of SnS by the reasonable Fe proportion. Therefore, in this work curiously focused to dope Fe with SnS. For the first time, Fe doped SnS thin film is successfully fabricated by NSP technique. The pure SnS structural, optical, morphological, and electrical properties were elaborately compared with different doping weight percentage using prepared Fe doped SnS (Fe:SnS). In addition, the prepared p-type behavior Fe:SnS thin film, which is coated on fluorine doped tin oxide (FTO), photovoltaics behavior is analyzed with the structure of FTO/n-CdS/p-Fe:SnS/Al and also their results are discussed in detail.

## 2 Experimental procedure

### 2.1 Growth of SnS and Fe:SnS thin film

The source chemicals such as tin chloride ( $\text{SnCl}_2 \cdot 2\text{H}_2\text{O}$ ), ferrous (II) chloride ( $\text{FeCl}_2 \cdot 4\text{H}_2\text{O}$ ) and thiourea ( $\text{CH}_4\text{N}_2\text{S}$ ) were used for NSP technique to prepare SnS and Fe:SnS thin films. The precursor's solution for  $\text{SnCl}_2 \cdot 2\text{H}_2\text{O}$  (0.1 M) and  $\text{CH}_4\text{N}_2\text{S}$  (0.1 M) were individually in beaker using deionized water and isopropanol in the ratio of 3:1. To prepare the bare SnS, the prepared solutions with equal volume were mixed together and were sprayed on substrate at 350 °C onto glass substrates. For the deposition of Fe:SnS, the different weight percentage (wt.%) such as 2, 4, 6, 8 and 10 wt.% using prepared solution was mixed with  $\text{SnCl}_2 \cdot 2\text{H}_2\text{O}$  source solution and then combined with  $\text{CH}_4\text{N}_2\text{S}$  solution in equal volume. Prior to the deposition, all the substrates were successively cleansed in water bath and then followed by conc. HCl and acetone. The solution flow rate and the carrier gas pressure can be controlled in the NSP technique. The deposition conditions like carrier gas pressure, flow rate and distance between the nozzle and substrate were kept as 2 kg/cm<sup>2</sup>, 2 ml/min and 5 cm, respectively. The microcontroller stepper motor was used to move the spray nozzle along X–Y plane, to maintain uniform coating all over the substrate. The deposited films were allowed to cool to reach room temperature slowly to increase the adhesion properties.

### 2.2 Characterization of SnS and Fe:SnS thin film

Film thickness of pure and Fe:SnS were measured using profile meter. XPERT-PRO X-ray diffractometer (XRD) was employed to investigate the structural properties with  $\text{CuK}_\alpha$  monochromatic radiation ( $\lambda = 1.5406$  nm). The Raman spectra were recorded by Princeton Acton SP 2500 at room temperature. The surface topography was visualized by using atomic force microscopy (AFM, Park Scientific Instruments

- Auto Probe CP). The optical studies were studied by Hitachi-330, UV visible spectrometer. Perkin Elmer LS55 fluorescence spectrophotometer was used to observe the photoluminescence properties in the range of 600–900 nm. The electrical resistivity was measured by Hall Effect measurement using four probe configurations.

### 2.3 Device fabrication

For the solar cell fabrication, n-type cadmium sulfide (CdS) layer was coated onto the prepared p-Fe:SnS layer by spray technique using cadmium chloride (0.1 mol/gm) and thiourea (0.1 mol/gm) mixed solution at the substrate temperature of 310 °C with the spray pressure of 0.5 Kg/cm<sup>2</sup>. The thickness of CdS layer was about 200 nm. The aluminum paste was used as dots to make the metal contacts. Finally, the typical structure of FTO/n-CdS/p-Fe:SnS/Al was prepared for photovoltaics. The current density (J)—voltage (V) measurements for the fabricated n-CdS/p-Fe:SnS heterojunction were performed using Keithley source meter 2450.

## 3 Results and discussion

### 3.1 Structural studies

Figure 1 shows the XRD profiles of pure and Fe:SnS thin films. The observed results revealed the polycrystalline nature with orthorhombic crystal structure for pure and Fe:SnS. The perceived peaks are well indexed with standard JCPDS (#75-2115) results. For pure SnS, (201), (111), (400), (211), (410), (411), (212) and (511) lattice planes are observed along with preferential orientation of (201) plane. The peak intensities are varied for different wt% using prepared Fe:SnS thin films. When the Fe:SnS film prepared using 6 wt% of Fe source, (400) lattice plane exhibited as a preferential orientation. Further increased the Fe doping to 10 wt%, (111) lattice is emerged as a preferential plane. The peak intensities and preferential orientation variations signifies the residual stress in the Fe:SnS film which caused by the doping of Fe with low ionic radius than Sn [26]. This result clearly indicates that Fe ions are interstitial position to near the Sn sites in the SnS lattice sites.

The full width at half maxima (FWHM) is considerably affected due to inclusion of Fe with SnS as given in Table 1 which can be affect the micro structural properties of Fe:SnS thin films [28]. The different micro structural parameters such as crystallites size, micro strain( $\epsilon$ ), dislocation density ( $\delta$ ) number of crystallites ( $n_c$ ) and texture coefficient ( $TC_{(hkl)}$ ) were estimated by the reported calculation method for pure and Fe:SnS thin films [29, 30]. The estimated micro structural values are provided in the Table 1. The crystallite size is observed at 16 nm for pure SnS and it has attained to

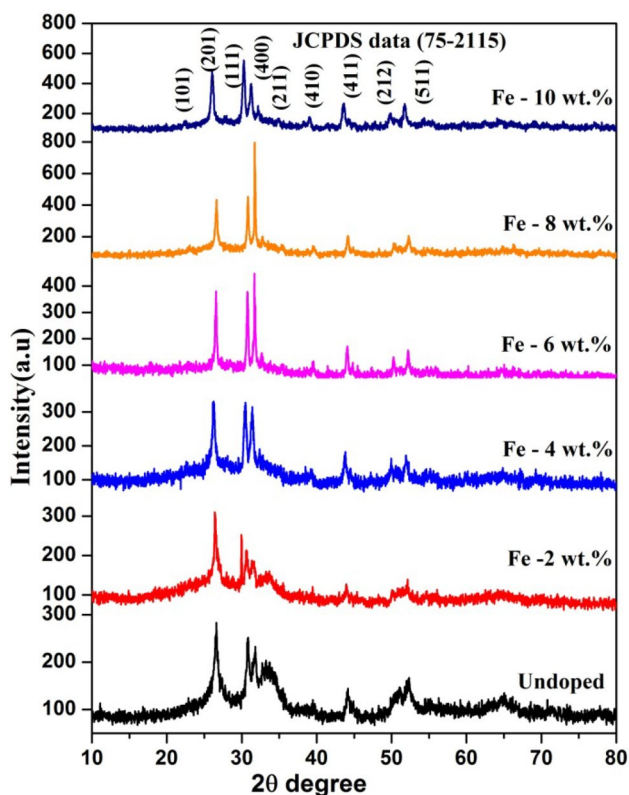


**Fig. 1** XRD spectra of undoped and different Fe doping weight percentage using prepared SnS films

74 nm for 8 wt.% using prepared Fe:SnS. The crystallite size values are increased linearly upto 8 wt.% of Fe:SnS and then decreased (~39 nm) for 10 wt.% due to deep alteration of SnS structure by larger amount Fe doping which is consistent with earlier result [31]. Similarly, the lattice imperfections of  $\epsilon$ ,  $\delta$  and  $n_c$  were noticed to decrease with increase of Fe doping upto 8 wt.% and then increased which attributes to the variation of crystallite sizes. The least values of  $\epsilon$ ,  $\delta$  and  $n_c$  for 8 wt.% using prepared Fe:SnS shows improvement of grain boundaries, which allows the free transport of charge carriers within the lattice. These results illustrated the role of doping on the micro structural properties of Fe:SnS.

**Table 1** Microstructural parameters of pure and Fe:SnS thin films

Fe doping weight percentage (wt%)	FWHM radian	Crystallite size (D) nm	Number of crystallites ( $n_c$ ) $\times 10^{17} \text{ m}^{-2}$	Dislocation density ( $\delta$ ) $\times 10^{15} \text{ lines/m}^2$	Micro strain ( $\epsilon$ ) $\times 10^{-3}$	Texture Coefficient (TC)	Thickness nm
0 (Pure)	0.52	16	1.91	3.98	2.16	1.051	757
2	0.29	28	0.36	1.27	1.23	1.167	782
4	0.23	37	0.17	0.73	0.93	1.305	834
6	0.17	49	0.08	0.42	0.71	1.328	879
8	0.11	74	0.02	0.18	0.46	1.413	914
10	0.21	39	0.16	0.64	0.87	1.331	854

Raman scattering used to confirm the structure by the lattice phonon modes [35]. Figure 2 shows the Raman spectra of pure SnS and Fe:SnS. Generally, SnS possess 24 vibrational modes for orthorhombic crystal structure with eight atoms per unit cell. The modes at the center of the Brillouin zone can be derived as,

$$\Gamma = 4A_g + 2B_{1g} + 4B_{2g} + 2B_{3g} + 2A_u + 4B_{1u} + 2B_{2u} + 4B_{3u} \quad (1)$$

Among them SnS has 21 optical phonon modes which comprised of twelve Raman active modes ( $4A_g$ ,  $2B_{1g}$ ,  $4B_{2g}$  and  $2B_{3g}$ ), seven infrared active modes ( $3B_{1u}$ ,  $1B_{2u}$  and  $3B_{3u}$ ) and two ( $2A_u$ ) inactive modes [32]. Pure and Fe doped SnS samples are exposed similar pattern of Raman profiles with the variation of the peak intensity. Raman peaks are located at 47, 70, 96, 117, 174 and 217  $\text{cm}^{-1}$  wave number. The exhibited low frequency at 47  $\text{cm}^{-1}$  and high frequency at 217  $\text{cm}^{-1}$  Raman positions are related to waving  $B_{3g}$  and the distorted NaCl structure  $A_g$  (LO) mode vibrations, respectively [33]. The Raman position at 70  $\text{cm}^{-1}$  is attributed to the combination of  $A_g$  and  $B_{2g}$  mode for orthorhombic phase SnS which is consistent with earlier report [34]. The Raman positions at 96, 117 and 174  $\text{cm}^{-1}$  wave number are related to  $A_g$  modes [33, 35]. The obtained results are well consistent with the XRD results.

The 2D and 3D atomic force micrographs (AFM) for pure and Fe:SnS films using different Fe doping concentrations are shown in Fig. 3(a-1). Topography images are clearly representing the surface modifications due to different Fe concentration using doped SnS. The smaller size grains are combined to form bigger grains. The surface roughness and grain size for pure and Fe doped SnS films are given in the Table 2. The maximum value of grain size is 89 nm using AFM for 8 wt% Fe doping consistent with XRD crystallite size results. The surface roughness is increased upto 8 wt% Fe doping and then decreased slightly which is due to variation of AFM grain sizes.

The energy dispersive spectroscopy results were used to confirm the inclusion of Fe into SnS matrix for Fe:SnS thin films. The composition of Sn, S and Fe elements in the pure and Fe:SnS films are given in Table 3. From the observed

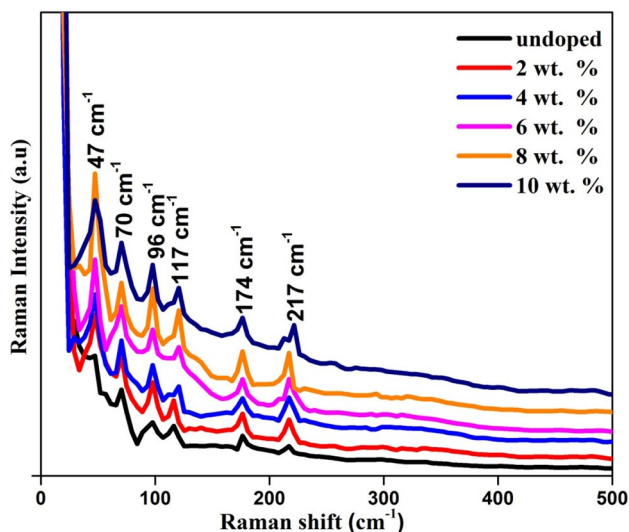


**Fig. 2** Raman spectra of undoped and different Fe doping weight percentage using prepared SnS films

result, Sn elemental percentage is decreased whereas Fe percentage is increased with increase of doping percentage with the constant value of S elemental percentage which confirmed the replacement of Sn by doped Fe ions.

### 3.2 Optical properties

The optical transmittance properties are evaluated through UV-Vis-NIR spectroscopy results for pure and Fe:SnS thin films. Figure 4 shows transmittance spectra of pure and Fe:SnS thin films. The pure SnS exposed better optical transmittance properties compared with their Fe doped results. Also, optical band edge shifted considerably towards visible region due to inclusion of Fe atoms into the SnS matrix. The maximum transmittance of 63% is observed for pure SnS, whereas it has declined to 15% for 8 wt% using prepared Fe:SnS. The optical properties variation can be directly related to crystallite size variation and lattice imperfection. The absorption coefficient ( $\alpha$ ) was estimated using transmission data by the following relation [36],

$$\alpha = \frac{\ln\left(\frac{1}{T}\right)}{t} \quad (2)$$

Where, ' $\alpha$ ' is an absorption coefficient, 't' is thickness of thin film and 'T' is the transmittance. The absorption coefficient variations against wavelength for pure and Fe:SnS thin films is shown in Fig. 5. The absorption coefficient value is increased with respect to Fe doping wt%, attained maximum for 8 wt. %Fe doping concentration and then decreased slightly for 10 wt% Fe concentration. The

observed absorption coefficient pattern directly reflects transmittance results. Hence, the prepared films have high absorption coefficient value which has the ability to absorb sunlight from the visible to near infrared region.

The optical energy band gap for pure and Fe:SnS thin films were determined by the relation(3) [18].

$$(\alpha h\nu)^n = B(h\nu - E_g) \quad (3)$$

Where B is proportionality constant, n is the index parameter which is involved in the transition process (direct or indirect) and  $E_g$  is the energy gap. Figure 6 shows Tauc's plot between  $(\alpha h\nu)^2$  and photon energy ( $h\nu$ ) for pure and Fe:SnS thin films. The optical band gap energy is extracted by the linear extrapolation to zero X-axis. For pure SnS, optical band gap is observed at 1.96 eV. When the Fe doped with SnS, band gap value is decreased with respect to Fe doping concentration upto 8 wt% and then increased for 10 wt%. The lower value of band gap is observed at 1.58 eV for Fe:SnS with 8 wt% Fe doping, which is very well agreed with the previous values [26, 37]. The observed energy band gap values are provided in the Table 2.

Figure 7 shows room temperature photoluminescence spectra for pure and prepared SnS thin films with the excitation wavelength ( $\lambda_{exc}$ ) of 350 nm. The strong emission band is observed at 709 nm for pure SnS. When the Fe atom incorporated into SnS matrix, the emission band is shifted to around 770 nm and their intensity is increased with increase of Fe doping percentage. The high intensity peak at 772 nm is observed Fe:SnS with 8 wt% Fe doping concentration. It can be created by increase of free excitons density, which represents recombination of electrons in CB and holes in VB in the Fe:SnS thin films [38, 39]. The observed emission peak at 772 nm, which is equal to 1.58 eV, contributes to the near band edge mission and consisted with optical band gap result [23]. For Fe higher doping wt.%, the emission peak is shifted to lower wavelength region.

### 3.3 Electrical properties

Electrical properties were evaluated for pure and Fe:SnS thin films by Hall effect measurement system. Figure 8 shows the electrical resistivity, hall mobility and carrier concentrations for the pure and Fe doped SnS with respect to different Fe doping wt.%. The carrier concentration is considerably increased due to addition of Fe into SnS matrix as shown in Fig. 8. Also, the substitution of Fe ions with SnS is considerably decreased the resistivity. Thus conductivity achieves at maximum at 18.04  $\text{cm}^2/\text{Vs}$  for Fe:SnS with 8 wt% Fe doping, whereas the lowest resistivity value observed at  $3.32 \times 10^{-2} \Omega \text{ cm}$ . The observed high conductivity is directly corresponding to the grain size which has elaborated in the previous section. The observed

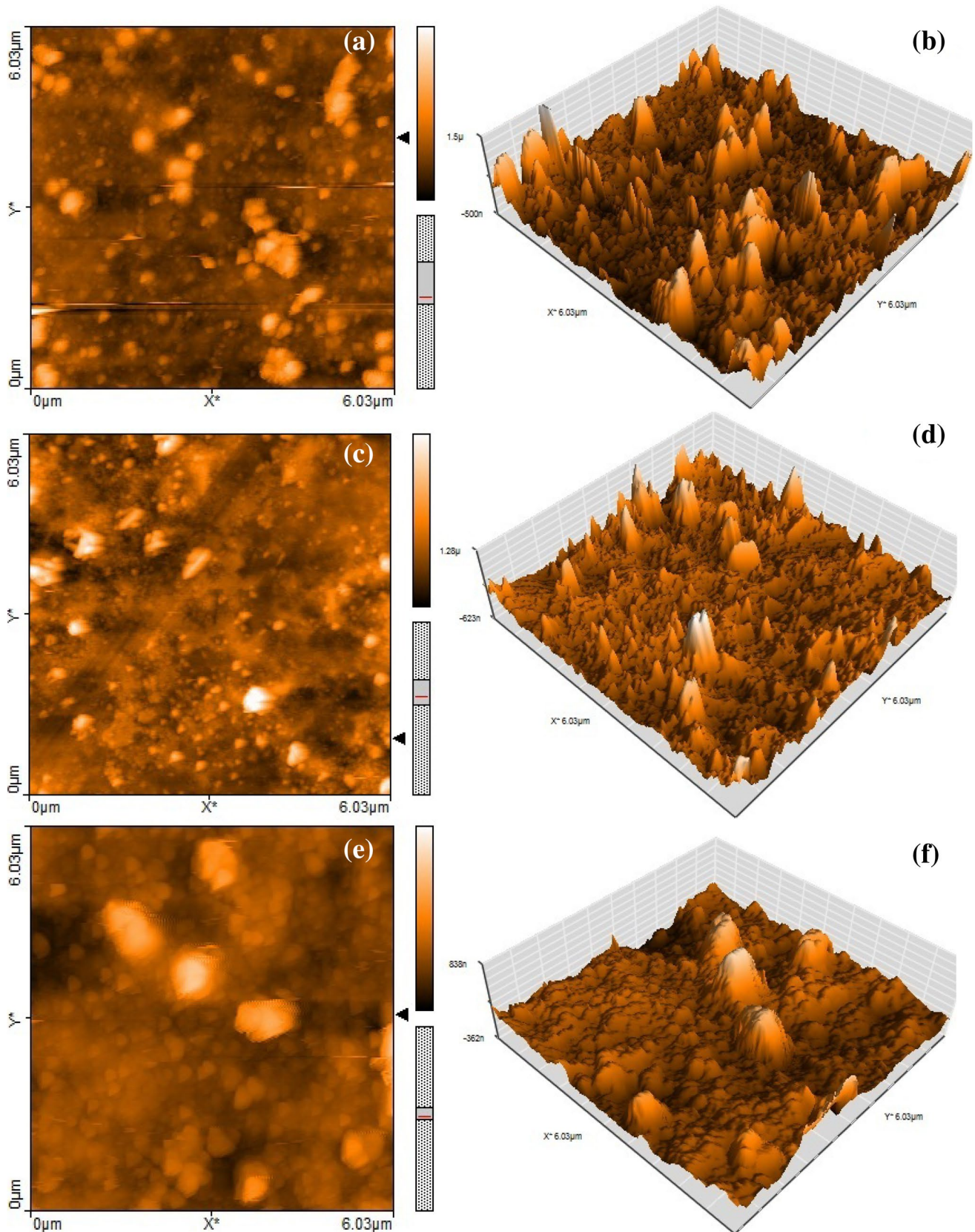


**Fig. 3** 2D and 3D view AFM image of **a, b** undoped and different Fe doping weight percentage **c, d** 2 wt%, **e, f** 4 wt%, **g, h** 6 wt%, **i, j** 8 wt% and **k, l** 10 wt% using prepared SnS films

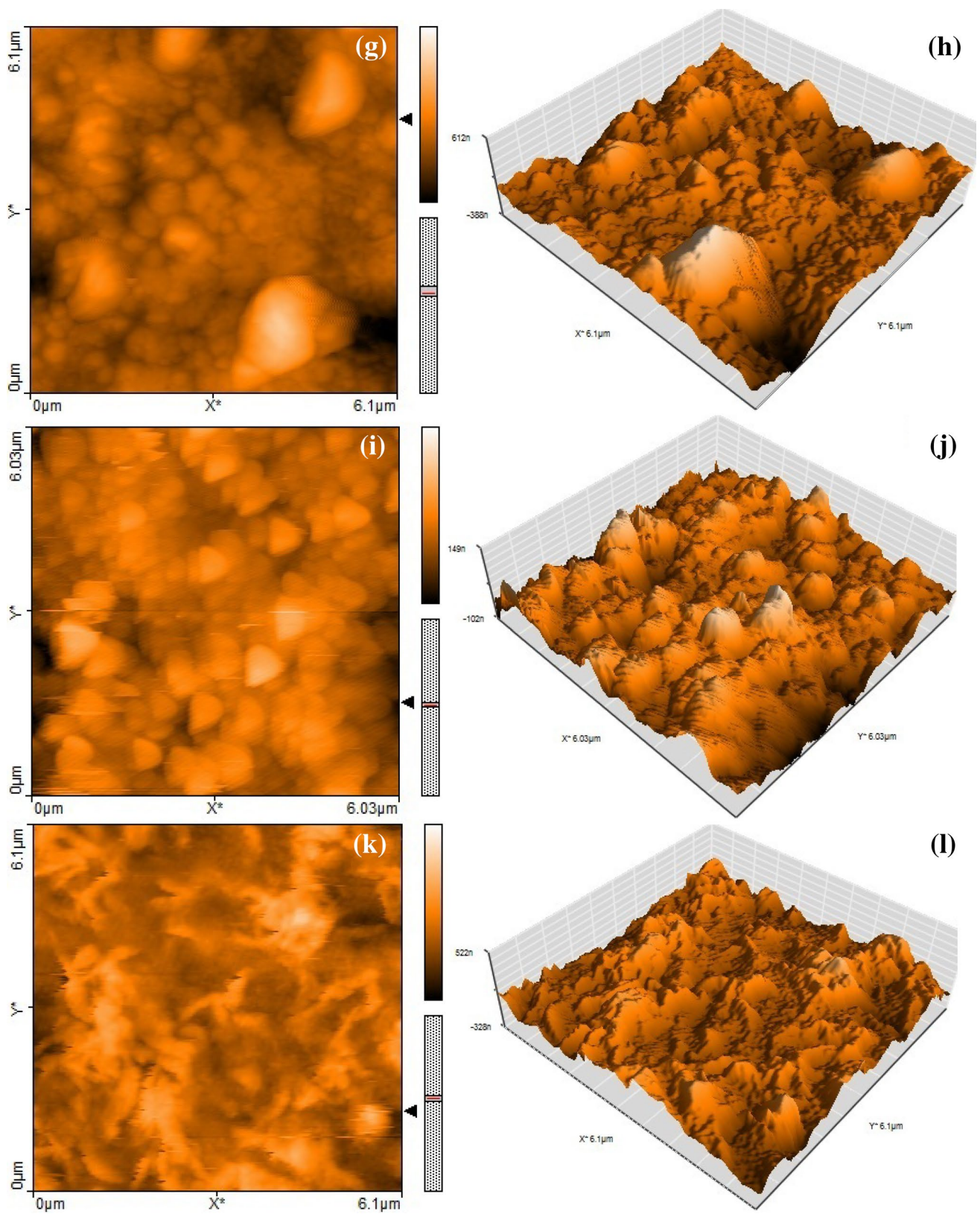


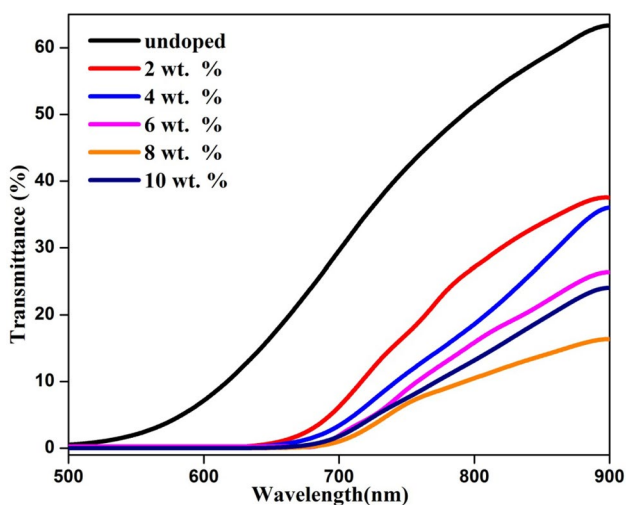
Fig. 3 (continued)

**Table 2** Surface roughness, grain size and band gap values of pure and Fe:SnS thin films

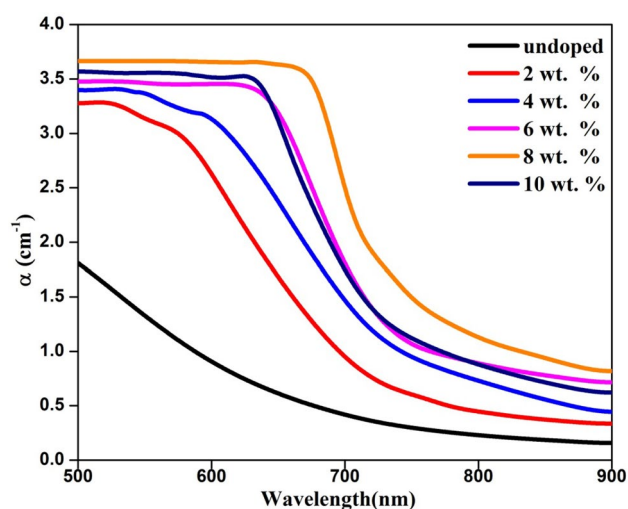
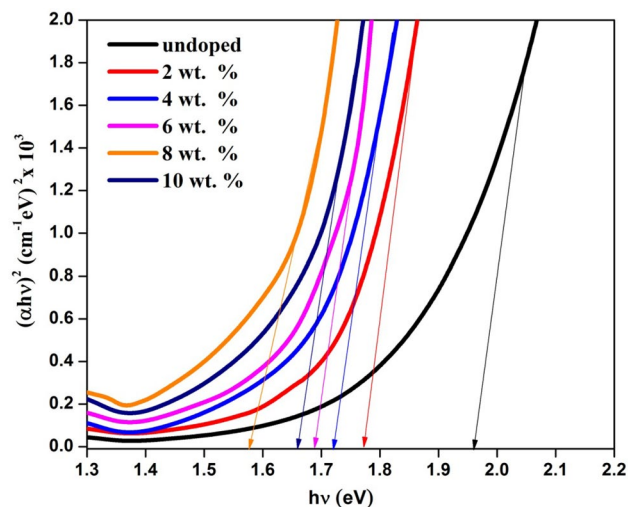
Fe doping weight percentage (wt%)	Surface Roughness (nm)	Grain Size (nm)	Energy gap (eV)
0 (Pure)	11	20	1.96
2	24	37	1.76
4	33	46	1.72
6	47	67	1.68
8	68	89	1.58
10	41	58	1.66

**Table 3** Elemental composition analysis of pure and Fe:SnS thin films

Fe doping (wt%)	Element (at%)		
	Sn	S	Fe
0 (Pure)	50.96	49.04	0
2	49.69	49.76	0.55
4	48.52	49.69	1.79
6	47.58	49.48	2.94
8	44.93	48.83	6.24
10	43.10	48.53	8.37

**Fig. 4** Transmittance spectra of undoped and different Fe doping weight percentage using prepared SnS films

electrical parameters are provided in the Table 4. For 10 wt% using prepared Fe:SnS, electrical parameters are contradictorily observed due to the vast variation of structure as described in structural section and decrement of phonon scattering mechanism [40, 41].

**Fig. 5** Absorption coefficient spectra of undoped and different Fe doping weight percentage using prepared SnS films**Fig. 6** Tauc's plot of undoped and different Fe doping weight percentage using prepared SnS films

### 3.4 I–V characteristics of n-CdS/p-Fe:SnS heterostructure

Based on our literature knowledge, at the first time n-CdS/p-Fe:SnS heterostructure is constructed by NSP technique for photovoltaics. For the preparation of FTO/n-CdS/p-Fe:SnS/Al, the optimized characteristic sample of Fe:SnS with 8 wt.% of Fe doping was employed to fabricate solar cell structure. The current–voltage (I–V) characteristics were analyzed at room temperature under the illumination of halogen lamp at 100 mW/cm<sup>2</sup>. Figure 9a shows I–V curve of prepared solar cell with the active area of 0.5 cm<sup>2</sup>. Under the dark, the minimum value of current is observed attributed to

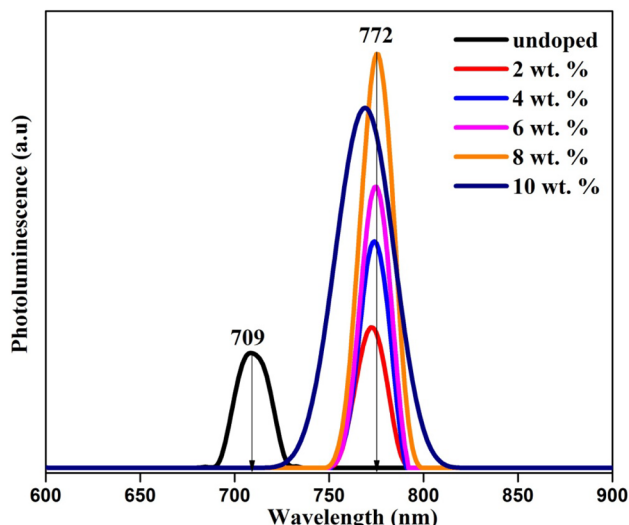


**Fig. 7** PL spectra of undoped and different Fe doping weight percentage using prepared SnS films

the minority carriers. When the illumination showered on the solar cell, the current value is increased due to production of charge carriers by incident photons [31].

Figure 9b shows the I–V characteristics of FTO/n-CdS/p-Fe:SnS/Al heterojunction under illumination. The open circuit voltage ( $V_{OC}$ ) and short circuit current ( $J_{SC}$ ) were determined from the I–V graph. The obtained  $J_{SC}$ ,  $V_{OC}$  and fill factor (FF) solar cell parameters values are at 1.96 mA  $cm^{-2}$ , 358 mV and 25.7%, respectively [40, 42]. The power conversion efficiency ( $\eta$ ) for our constructed solar cell structure is estimated to be 0.18% [37]. The observed performance is given a path to fabricate the solar cell structure with simple and cost effective methodologies. However, it

**Fig. 8** The variation of resistivity, carrier concentration and mobility for undoped and Fe doped SnS films

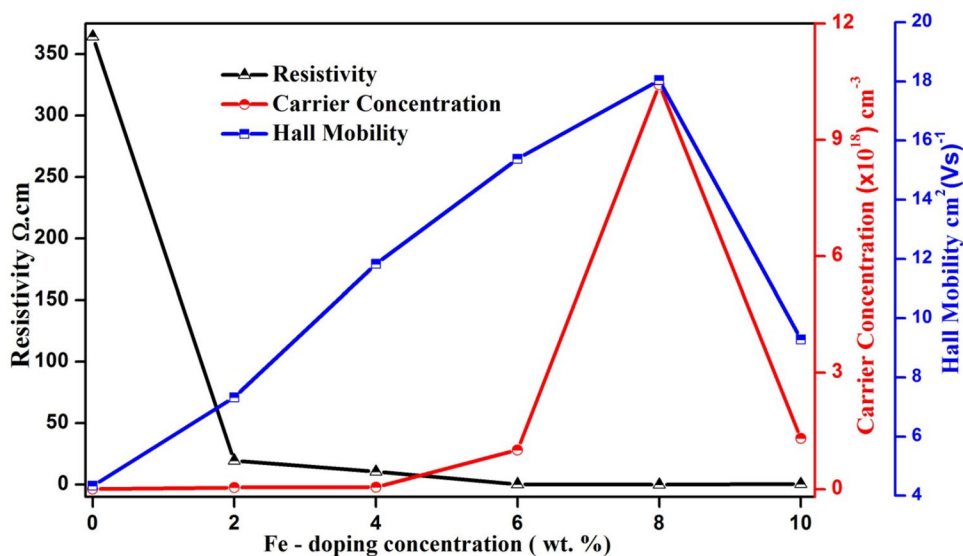


**Table 4** Electrical parameters of pure and Fe:SnS thin films

Fe doping weight percentage (wt%)	Resistivity $\Omega cm$	Carrier concentration $cm^{-3}$	Hall mobility $cm^2 /Vs$
0 (Pure)	$3.64 \times 10^2$	$3.95 \times 10^{15}$	4.33
2	$1.95 \times 10^1$	$4.36 \times 10^{16}$	7.32
4	$1.05 \times 10^1$	$5.04 \times 10^{16}$	11.83
6	$4.02 \times 10^{-1}$	$1.01 \times 10^{18}$	15.38
8	$3.32 \times 10^{-2}$	$1.04 \times 10^{19}$	18.04
10	$5.13 \times 10^{-1}$	$1.31 \times 10^{18}$	9.28

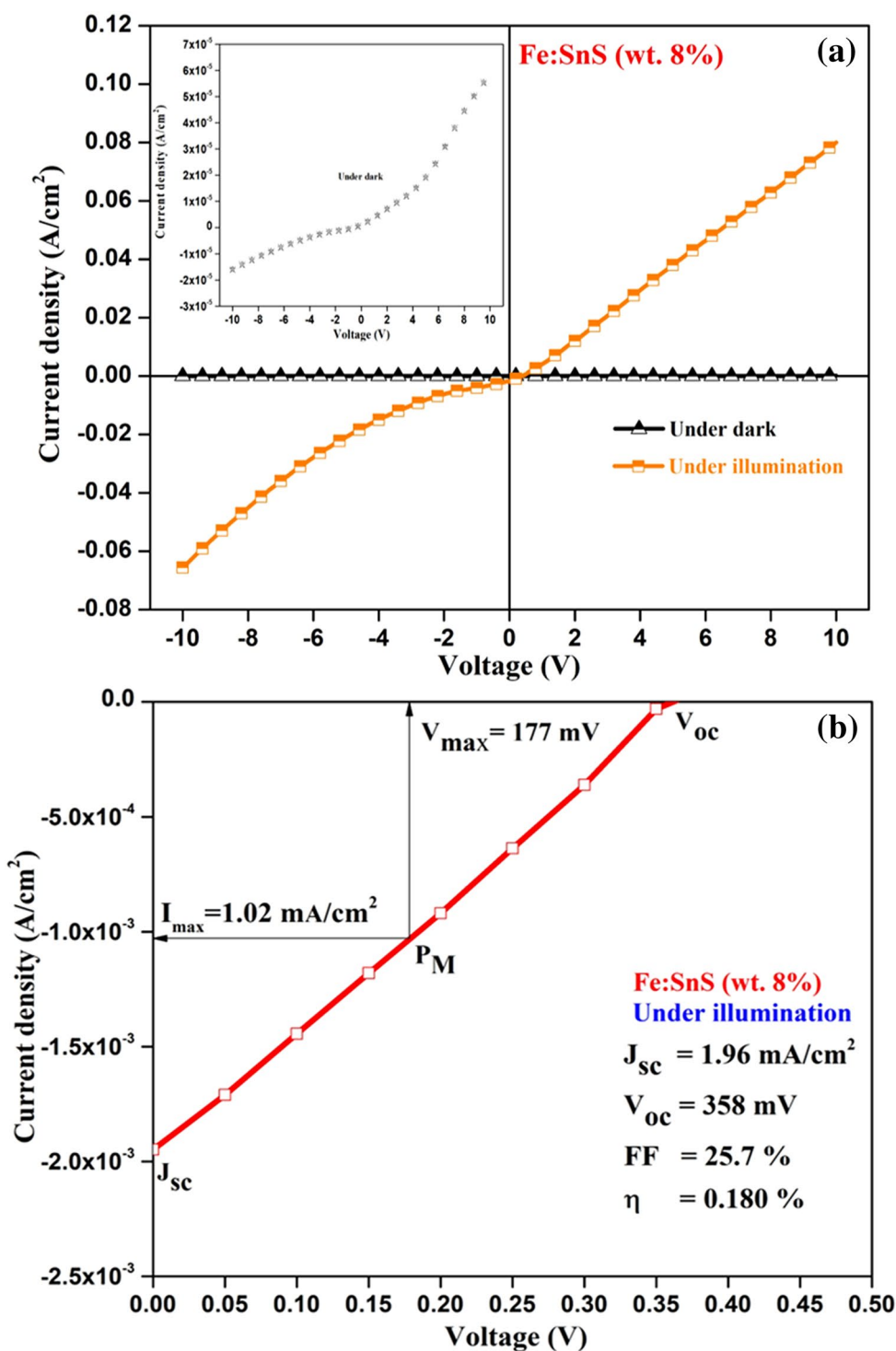
will further tune to achieve maximum by different metal doping and annealing.

### 4 Conclusions

Pure and Fe doped SnS thin films were deposited by NSP technique with different Fe doping wt% (2 to 10 wt%). The detailed studies were carried out for their structural, optical and electrical properties. XRD results clearly picturized the structure variation due to inclusion of Fe atom into SnS matrix. Raman results confirmed the orthorhombic structured SnS phase for pure and Fe:SnS thin films. Topological properties were demonstrated by AFM images. Optical properties proved the visible region transmittance properties for Fe:SnS thin films and exhibited the low band gap of 1.58 eV for 8 wt% using prepared Fe:SnS film. Near band edge luminescence signal exhibited at 772 nm for optimized doping concentration using prepared Fe:SnS. The low resistivity and high carrier



**Fig. 9** **a** I–V characteristics under dark and illumination for FTO/n-CdS/p-Fe:SnS heterostructure (inset—expanded view for dark I–V characteristics); **b** selective portion of I–V characteristics for FTO/n-CdS/p-Fe:SnS heterostructure under illumination



concentration values were achieved at  $3.32 \times 10^{-2} \Omega \text{ cm}$  and  $1.04 \times 10^{19} \text{ cm}^{-3}$ , respectively for 8 wt.% using prepared Fe:SnS film. The prepared FTO/n-CdS/p-Fe:SnS/Al heterojunction structure, at first time by NSP method, unveiled the efficiency of 0.18%. The observed results proved their suitability to construct photovoltaic devices

using NSP prepared samples and it will be achieved by different modification the better efficiency for future energy application.

**Acknowledgements** The authors extend their appreciation to the Deanship of Scientific Research at King Khalid University for funding

this work through General Research Project under grant number (R.G.P.1/45/39). This work was also partly supported by the Basic Science Research Program through the National Research Foundation of Korea (NRF) funded by the Ministry of Education (No. 2017R1D1A1A09000823).

## References

- N.P. Klochko, O.V. Lukianova, V.R. Kopach, I.I. Tyukhov, N.D. Volkova, G.S. Khrypunov, V.M. Lyubov, M.M. Kharchenko, M.V. Kirichenko, Development of a new thin film composition for SnS solar cell. *Sol. Energy* **134**, 156–164 (2016)
- F. Ballipinar, A.C. Rastogi, Tin sulfide (SnS) semiconductor photo-absorber thin films for solar cells by vapor phase sulfurization of Sn metallic layers using organic sulfur source. *J. Alloy. Compd.* **728**, 179–188 (2017)
- S. Di Mare, D. Menossi, A. Salavei, E. Artegiani, F. Piccinelli, A. Kumar, G. Mariotto, A. Romeo, SnS thin film solar cells: perspectives and limitations. *Coatings* **7**(2), 34 (2017)
- D. Avellaneda, G. Delgado, M.T.S. Nair, P.K. Nair, Structural and chemical transformations in SnS thin films used in chemically deposited photovoltaic cells. *Thin Solid Films* **515**(15), 5771–5776 (2007)
- M. Parenteau, C. Carlone, Influence of temperature and pressure on the electronic transitions in SnS and SnSe semiconductors. *Phys. Rev. B* **41**(8), 5227–5234 (1990)
- Y. Aimi, K. Takashi, A. Yoji, N. Shigeyuki, O. Hiroto, K. Hironori, A. Hideaki, Influence of Sn/S composition ratio on SnS thin-film solar cells produced via co-evaporation method. *Jpn. J. Appl. Phys.* **57**(2S2), 02CE08 (2018)
- H. Noguchi, A. Setiyadi, H. Tanamura, T. Nagatomo, O. Omoto, Characterization of vacuum-evaporated tin sulfide film for solar cell materials. *Sol. Energy Mater. Sol. Cells* **35**, 325–331 (1994)
- Y. Zou, Y. Wang, Microwave solvothermal synthesis of flower-like SnS<sub>2</sub> and SnO<sub>2</sub> nanostructures as high-rate anodes for lithium ion batteries. *Chem. Eng. J.* **229**, 183–189 (2013)
- X. Jiang, X. Yang, Y. Zhu, J. Shen, K. Fan, C. Li, In situ assembly of graphene sheets-supported SnS<sub>2</sub> nanoplates into 3D macroporous aerogels for high-performance lithium ion batteries. *J. Power Sources* **237**, 178–186 (2013)
- S. Weidong, H. Lihua, W. Haishui, Z. Hongjie, Y. Jianhui, W. Pinghui, Hydrothermal growth and gas sensing property of flower-shaped SnS<sub>2</sub> nanostructures. *Nanotechnology* **17**(12), 2918 (2006)
- W. Anaf, O. Schalm, K. Janssens, K. De Wael, Understanding the (in)stability of semiconductor pigments by a thermodynamic approach. *Dyes Pigm.* **113**, 409–415 (2015)
- K. Hartman, J.L. Johnson, M.I. Bertoni, D. Recht, M.J. Aziz, M.A. Scarpulla, T. Buonassisi, SnS thin-films by RF sputtering at room temperature. *Thin Solid Films* **519**(21), 7421–7424 (2011)
- M. Devika, N.K. Reddy, K. Ramesh, V. Ganesan, E. Gopal, K.R. Reddy, Influence of substrate temperature on surface structure and electrical resistivity of the evaporated tin sulphide films. *Appl. Surf. Sci.* **253**(3), 1673–1676 (2006)
- A. Tanuševski, D. Poelman, Optical and photoconductive properties of SnS thin films prepared by electron beam evaporation. *Solar Energy Mater. Solar Cells* **80**(3), 297–303 (2003)
- C. Gao, H. Shen, L. Sun, H. Huang, L. Lu, H. Cai, Preparation of SnS films with zinc blende structure by successive ionic layer adsorption and reaction method. *Mater. Lett.* **64**(20), 2177–2179 (2010)
- C. Gao, H. Shen, Influence of the deposition parameters on the properties of orthorhombic SnS films by chemical bath deposition. *Thin Solid Films* **520**(9), 3523–3527 (2012)
- V. Dhanasekaran, T. Mahalingam, J.K. Rhee, J. Chu, Bath temperature effects on the microstructural and morphological properties of SnS thin films. *J. Adv. Microsc. Res.* **6**(2), 126–130 (2011)
- K.D.A. Kumar, S. Valanarasu, K. Jeyadheepan, H.-S. Kim, D. Vikraman, Evaluation of the physical, optical, and electrical properties of SnO<sub>2</sub>:F thin films prepared by nebulized spray pyrolysis for optoelectronics. *J. Mater. Sci.: Mater. Electron.* **29**(5), 3648–3656 (2018)
- V. Gremenok, V.Y. Rud, Y.V. Rud, S. Bashkirov, V. Ivanov, Photosensitive thin-film In/p-Pb x Sn 1—x S Schottky barriers: fabrication and properties. *Semiconductors* **45**(8), 1053 (2011)
- S. Zhang, S.Y. Cheng, H.J. Jia, H.F. Zhou, Preparation and characterization of aluminium-doped SnS thin films. *Adv. Mater. Res.* **418–420**, 712–716 (2012)
- A. Akkari, M. Reghima, C. Guasch, N. Kamoun-Turki, Effect of copper doping on physical properties of nanocrystallized SnS zinc blend thin films grown by chemical bath deposition. *J. Mater. Sci.* **47**(3), 1365–1371 (2012)
- M. Devika, N.K. Reddy, K. Ramesh, K. Gunasekhar, E. Gopal, K.R. Reddy, Low resistive micrometer-thick SnS: Ag films for optoelectronic applications. *J. Electrochem. Soc.* **153**(8), G727–G733 (2006)
- K. Santhosh Kumar, C. Manoharan, S. Dhanapandian, A. Gowri Manohari, Effect of Sb dopant on the structural, optical and electrical properties of SnS thin films by spray pyrolysis technique. *Spectrochim. Acta Part A* **115**, 840–844 (2013)
- M. Reghima, A. Akkari, C. Guasch, N. Kamoun-Turki, Effect of indium doping on physical properties of nanocrystallized SnS zinc blend thin films grown by chemical bath deposition. *J. Renew. Sustain. Energy* **4**(1), 011602 (2012)
- M. Han, X. Zhang, Z. Zeng, The investigation of transition metal doped CuGaS<sub>2</sub> for promising intermediate band materials. *RSC Adv.* **4**(107), 62380–62386 (2014)
- A. Javed, A. Qurat ul, M. Bashir, Controlled growth, structure and optical properties of Fe-doped cubic  $\pi$ -SnS thin films. *J. Alloy. Compd.* **759**, 14–21 (2018)
- C. Rockstuhl, S. Fahr, F. Lederer, Surface plasmon polaritons in metallic nanostructures: Fundamentals and their application to thin-film solar cells. In *Next Generation of Photovoltaics*. (Springer, New York, 2012) pp. 131–155
- A.G. Manohari, S. Dhanapandian, C. Manoharan, K.S. Kumar, T. Mahalingam, Effect of doping concentration on the properties of bismuth doped tin sulfide thin films prepared by spray pyrolysis. *Mater. Sci. Semicond. Process.* **17**, 138–142 (2014)
- S. Thiagarajan, A. Sanmugam, D. Vikraman (2017) Facile Methodology of Sol–Gel Synthesis for Metal Oxide Nanostructures. In *Recent Applications in Sol–Gel Synthesis*, Ed. Usha Chandra, InTechOpen. <https://doi.org/10.5772/intechopen.68708>
- V. Dhanasekaran, T. Mahalingam, R. Chandramohan, J.-K. Rhee, J.P. Chu, Electrochemical deposition and characterization of cupric oxide thin films. *Thin Solid Films* **520**(21), 6608–6613 (2012)
- M. Reghima, A. Akkari, C. Guasch, M. Castagné, N. Kamoun-Turki, Synthesis and characterization of Fe-doped SnS thin films by chemical bath deposition technique for solar cells applications. *J. Renew. Sustain. Energy* **5**(6), 063109 (2013). <https://doi.org/10.1063/1.4830256>
- T.S. Reddy, M.S. Kumar, Effect of substrate temperature on the physical properties of co-evaporated Sn<sub>2</sub>S<sub>3</sub> thin films. *Ceram. Int.* **42**(10), 12262–12269 (2016)
- M. Li, Y. Wu, T. Li, Y. Chen, H. Ding, Y. Lin, N. Pan, X. Wang, Revealing anisotropy and thickness dependence of Raman spectra for SnS flakes. *RSC Adv.* **7**(77), 48759–48765 (2017)
- D. Vikraman, S. Thiagarajan, K. Karuppasamy, A. Sanmugam, J.-H. Choi, K. Prasanna, T. Maiyalagan, M. Thaiyan, H.-S. Kim, Shape- and size-tunable synthesis of tin sulfide thin films for

- energy applications by electrodeposition. *Appl. Surf. Sci.* **479**, 167–176 (2019)
35. S. Sohila, M. Rajalakshmi, C. Ghosh, A.K. Arora, C. Muthamizhchelvan, Optical and Raman scattering studies on SnS nanoparticles. *J. Alloy. Compd.* **509**(19), 5843–5847 (2011)
  36. T. Mahalingam, V. Dhanasekaran, G. Ravi, S. Lee, J.P. Chu, H.J. Lim, Effect of deposition potential on the physical properties of electrodeposited CuO thin films. *J. Optoelectron. Adv. Mater.* **12**(6), 1327–1332 (2010)
  37. O.V. Bilousov, Y. Ren, T. Törndahl, O. Donzel-Gargand, T. Ericson, C. Platzer-Björkman, M. Edoff, C. Hägglund, Atomic layer deposition of cubic and orthorhombic phase tin monosulfide. *Chem. Mater.* **29**(7), 2969–2978 (2017)
  38. G. Kaur, A. Mitra, K.L. Yadav, Pulsed laser deposited Al-doped ZnO thin films for optical applications. *Progr. Nat. Sci.* **25**(1), 12–21 (2015)
  39. S. Gedi, V.R. Minnam Reddy, C. Park, J. Chan-Wook, K.T RR, Comprehensive optical studies on SnS layers synthesized by chemical bath deposition. *Opt. Mater.* **42**, 468–475 (2015)
  40. E. Shanthi, V. Dutta, A. Banerjee, K.L. Chopra (1980) Electrical and optical properties of undoped and antimony-doped tin oxide films. *J. Appl. Phys.* **51**(12):6243–6251
  41. B. Joseph, P.K. Manoj, V.K. Vaidyan, Studies on the structural, electrical and optical properties of Al-doped ZnO thin films prepared by chemical spray deposition. *Ceram. Int.* **32**(5), 487–493 (2006)
  42. M. Patel, A. Ray, Magnetron sputtered Cu doped SnS thin films for improved photoelectrochemical and heterojunction solar cells. *RSC Adv.* **4**(74), 39343–39350 (2014)

**Publisher's Note** Springer Nature remains neutral with regard to jurisdictional claims in published maps and institutional affiliations.